Enhanced Carrier Injection in AlGaN-Based Deep Ultraviolet Light-Emitting Diodes by Polarization Engineering at the LQB/p-EBL Interface

Mengran Liu and Chao Liu

***Abstract*—The external quantum efficiency (EQE) of AlGaN-based deep ultraviolet light-emitting diodes (DUV LEDs) is still far from satisfactory due to the main issues of electron leakage and insufficient hole injection. The positive sheet charges generated by polarization at the interface between the last quantum barrier (LQB) and the p-type electron blocking layer (p-EBL) can induce electron accumulation and hole depletion in the vicinity of this interface, leading to electron leakage and hindering the hole injection. In this paper, we propose an Al-composition-increasing AlGaN layer (ACI-AlGaN) inserted between the LQB and p-EBL to enhance the carrier injection ability of DUV LEDs via modulating the sheet charges generated by polarization at the LQB/EBL interface and the underlying mechanism was analyzed by numerical calculation. The inserted structure can eliminate the positive sheet charges at the p-side interface of LQB and induce hole accumulation in the vicinity of the n-side interface of p-EBL, which can subsequently reduce electron leakage and favor hole injection respectively. The proposed DUV LED structure with an ACI-AlGaN layer exhibited enhanced EQE by 45.7% and its forward voltage maintained undegraded. This design scheme can provide an alternative way to promote the performance of DUV LEDs with a variety of applications.**

***Index Terms*—Carrier injection, DUV LED, polarization-induced sheet charges.**

I. Introduction

THE need for phototherapy, medical diagnostics, water/air disinfection and purification, plant cultivation, communication and lithography in daily life and industrial community has given rise to increasing demands for high reliability, energy-efficient, and compact deep ultraviolet (DUV) light sources. Hitherto, mercury lamps have been the most commonly used DUV light sources, yet they are delicate, massive, toxic, and need long warm-up time. By contrast, AlGaN-based deep ultraviolet light-emitting diodes (DUV LEDs) featured with energy-saving, miniaturization, high reliability, and no damage to environment, exhibit great potential to replace mercury lamps [1]–[4]. In spite of some outcomes in AlGaN material growth processes and device structure devise strategies [5]–[13], the performance of AlGaN-based DUV LEDs still offers reasonable room for advancement. In most cases, the external quantum efficiency (EQE) of AlGaN-based DUV LEDs is less than 10% and the efficiency droop phenomenon is quite severe [14], [15]. It has been reported that electron leakage and the insufficient hole injection are two crucial factors hindering the improvement of the optical and electrical properties of DUV LEDs [1], [16]. In order to suppress the electron leakage, a p-type electron blocking layer (p-EBL) is commonly grown between the last quantum barrier (LQB) and the hole supplier layer [1], [17]. However, the issue of lattice mismatch is introduced because the Al mole fractions of LQB and p-EBL are commonly different and thus induce positive sheet charges by polarization at LQB/p-EBL interface, which is detrimental to hole injection [18]. Therefore, the LQB/p-EBL interface needs to be modified for the purpose of enhancing the EQE and optical power of DUV LEDs. Single AlN layer [19] and ultrathin AlGaN/AlInN heterojunction [20] inserted between the LQB and p-EBL were proposed to enhance hole injection by utilizing intraband tunneling process for holes. Refs [21]–[23] reported that introducing AlGaN/AlGaN superlattice insertion layer at the LQB/p-EBL interface can increase the effective barrier height for electrons and decrease the effective barrier height for holes. However, the aforementioned structures place high demands on precise control of epitaxial process for AlGaN-based DUV LEDs. Kolbe *et al.* [24] experimentally demonstrated that an electron blocking heterostructure (EBH) can effectively boost the luminous efficiency, which was attributed to the alleviated electron leakage and boosted hole injection with an Al-rich AlGaN insertion layer between the LQB and p-EBL. However, the underlying mechanism behind the enhanced carrier injection and confinement remains to be explored.

In this paper, we numerically analyzed the physical mechanism behind the enhancement of the carrier injection efficiency from the aspect of interface polarization to pave a way towards devising an elaborate device structure and achieving DUV LEDs with excellent performance. Furthermore, we propose an Al-composition-increasing AlGaN layer (ACI-AlGaN) inserted between the LQB and p-EBL to improve the carrier injection capability of DUV LEDs via modulating the interface

Manuscript received February 16, 2022; revised March 30, 2022; accepted April 1, 2022. Date of publication April 5, 2022; date of current version May 5, 2022. This work was supported in part by the Shenzhen Science and Technology Program under Grant JCYJ20210324141212030, in part by the Guangdong Basic and Applied Basic Research Foundation under Grant 2020A1515111018, in part by Shandong Provincial Natural Science Foundation under Grant ZR2020QF079, and in part by the Qilu Young Scholar Program under Grant 11500089963075. *(Corresponding author: Chao Liu.)*

The authors are with the School of Microelectronics, Institute of Novel Semiconductors, Shandong Technology Center of Nanodevices and Integration, State Key Laboratory of Crystal Materials, Shandong University, Jinan 250100, China and also with the Shenzhen Research Institute, Shandong University, Shenzhen 518057, China (e-mail: chao.liu@sdu.edu.cn).

Digital Object Identifier 10.1109/JPHOT.2022.3165036

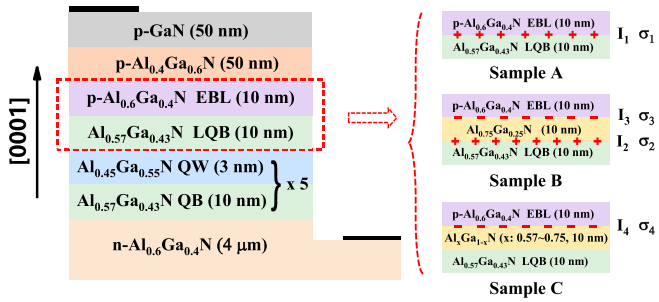

Fig. 1. Schematic structures and different polarization profiles between the LQB and p-EBL of Sample A, Sample B, and Sample C. Note that σ_1, σ_2, σ_3, and σ_4 represent different densities of sheet charges at the LQB/p-EBL interface (I_1), LQB/$Al_{0.75}Ga_{0.25}N$ interface (I_2), $Al_{0.75}Ga_{0.25}N$/p-EBL interface (I_3) and ACI AlGaN/p-EBL interface (I_4), respectively.

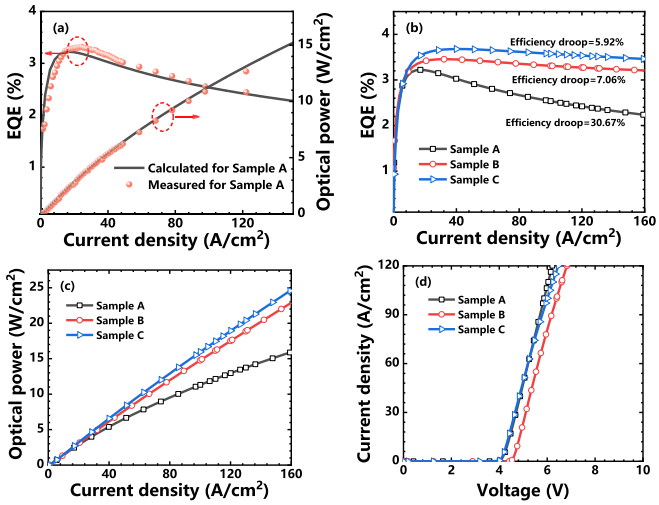

Fig. 2. (a) Calculated EQE and optical power as a function of the injection current density for Sample A. Measured EQE and optical power are also displayed. Calculated (b) EQE, (c) optical power, and (d) I-V characteristics for all the studied samples. Note that the values of efficiency droop of all samples are marked in Fig. 2(b).

sheet charges between the LQB and p-EBL, which can avoid introducing the issue of abrupt lattice mismatch between the LQB and the inserted structure and sustain undegraded forward voltage. Besides, the growth of the Al-graded AlGaN insertion layer is a well-developed epitaxy procedure by MOCVD [25], [26], and it will not bring extra complexity to the epitaxial process of the proposed structures. The proposed DUV LED with an ACI-AlGaN layer exhibited enhanced EQE by 45.7% at an injection current density of 120 A/cm^2, and the efficiency droop has also been alleviated significantly. The proposed device structure design strategy holds reasonable promise for achieving high efficiency and non-toxic DUV light sources to be applied in medical and biological fields, and disinfection/purification applications in everyday life.

II. Device Structure and Parameters

The AlGaN-based DUV LED structure reported by Zhang *et al.* [27] was used as the reference device (denoted as Sample A) in this study. Fig. 1 displays the schematic structures of the reference DUV LED and the proposed DUV LEDs (Sample B and Sample C). The reference device consists of a 4 μm-thick n-$Al_{0.6}Ga_{0.4}N$, whose electron concentration is 8×10^{18} cm^{-3}, followed by multiple quantum wells (MQWs), including five 3 nm-thick $Al_{0.45}Ga_{0.55}N$ quantum wells separated by six 10 nm- thick $Al_{0.57}Ga_{0.43}N$ quantum barriers. On the top of the MQW region is a 10 nm-thick p-type $Al_{0.6}Ga_{0.4}N$ electron blocking layer followed by a 50 nm-thick p-$Al_{0.4}Ga_{0.6}N$ hole supplier layer and a 50 nm-thick p-GaN. The effective hole concentrations of the p-type layers are set to $\sim 1 \times 10^{17}$ cm^{-3}. Except for the identical epitaxial structure to Sample A, Sample B and Sample C possess a 10 nm-thick unintentionally doped $Al_{0.75}Ga_{0.25}N$ layer and ACI-$Al_xGa_{1-x}N$ ($x = 0.57 \sim 0.75$) layer between the LQB and p-EBL, respectively, as shown in Fig. 1. All the investigated DUV LEDs have a mesa size of 350 μm $\times$ 350 μm.

We conducted the numerical investigations on the optical and electrical properties of DUV LEDs by utilizing the Advanced Physical Models of Semiconductor Devices (APSYS) software, which can self-consistently solve Schrödinger equation, Poisson's equation, current continuity equation, and drift-diffusion equation [28], [29]. In the simulation procedure, the Shockley-Read-Hall (SRH) recombination lifetime, Auger recombination coefficient and light extraction efficiency (LEE) were set to 14 ns [30], 1.7×10^{-30} cm^6/s [30], [31], and 6% [27], [32], respectively. These three parameters were determined by the fitting process of the calculated and measured EQE and optical power of the reference device, as shown in Fig. 2(a). The band offset ratio of AlGaN/AlGaN heterojunctions was set to be 0.5/0.5 [33] for the purpose of characterizing energy band diagrams of the studied DUV LEDs.

III. Results and Discussion

The calculated EQE and optical power of all the devices are presented in Fig. 2(b) and (c), respectively. Sample B exhibits obviously enhanced EQE and light output optical power compared to Sample A. The efficiency droop is reduced from 30.67% for Sample A to 7.06% for Sample B. As for Sample C, both the EQE and optical power are further improved in contrast to Sample B. In addition, the efficiency droop of Sample C is reduced to 5.92%. Fig. 2(d) displays the I-V characteristics of all the investigated samples. It can be observed that the forward voltage of Sample B is 0.42 V larger than that of Sample A, while Sample C exhibits nearly identical forward voltage as Sample A under an injection current density of 10 A/cm^2. The increment of forward voltage for Sample B can be attributed to the extra electrical resistance of the AlGaN insertion layer with a reasonably high Al composition, as experimentally demonstrated in [24]. Therefore, the implementation of an Al-rich and linearly-increasing AlGaN layer between the LQB and the EBL can obtain enhanced EQE and optical power of DUV LEDs, meanwhile not degrading the forward voltage.

To illustrate the physical mechanism behind the performance enhancement of the proposed devices, we plotted the calculated energy band diagrams of Sample A, Sample B, and Sample

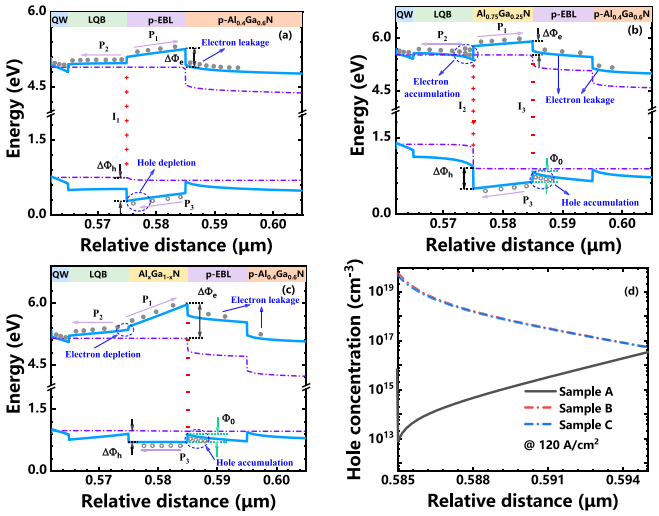

Fig. 3. Calculated energy band diagrams of (a) Sample A, (b) Sample B, and (c) Sample C under an injection current density of 120 A/cm^2. Note that "+", "-", gray solid balls and gray circles represent positive sheet charges, negative sheet charges, electrons, and holes, respectively, as shown in Fig. 3(a), (b) and (c). And process P_1, P_2, and P_3 denote electron overflowing, electron being reflected, and hole traveling from p-type region into the MQW region. Besides, $\Delta\Phi_e$, $\Delta\Phi_h$, and Φ_0 represent the effective barrier height for electrons, the effective barrier height for holes and the barrier height at the inserted $Al_xGa_{1-x}N$/p-EBL interface, respectively. (d) The hole concentration in p-EBL of all samples at 120 A/cm^2. Note that the hole concentration of Sample A is artificially shifted by 10 nm to make a clear comparison as the relative distance of p-EBL in Sample A is 10 nm lower than that in the proposed devices.

C, as shown in Fig. 3(a), (b) and (c). The introduction of the AlGaN insertion layer for Sample B and Sample C will induce the generation of the sheet charges at heterointerfaces related to the insertion layer because of the existence of spontaneous polarization and piezoelectric polarization in AlGaN alloys. The density of sheet charges can be calculated through the approach reported by Fiorentini *et al.* [34] in the simulation process. According to the method, the spontaneous polarization of $Al_xGa_{1-x}N$ ternary alloy, in C/m^2, can be expressed as

$$P_{sp} = -0.09x - 0.034\,(1-x) + 0.019x \tag{1}$$

in which x is the Al mole fraction of $Al_xGa_{1-x}N$ ternary alloy. As for the piezoelectric polarization of $Al_xGa_{1-x}N$ layer, the strain needs to be considered under the circumstance of pseudomorphic growth. And the piezoelectric polarization can be expressed as a Vegard interpolation of the bulk piezoelectric polarization of AlN and GaN binary alloy (P_{pz}^{AlN} and P_{pz}^{GaN}) in terms of strain $\varepsilon(x)$, in C/m^2:

$$P_{pz} = xP_{pz}^{AlN}\left[\varepsilon\left(x\right)\right] + (1-x)\,P_{pz}^{GaN}\left[\varepsilon\left(x\right)\right] \tag{2}$$

in which $P_{pz}^{AlN}[\varepsilon(x)]$ and $P_{pz}^{GaN}[\varepsilon(x)]$ can be derived from the following equations:

$$P_{pz}^{AlN} = -1.808\varepsilon\left(x\right) + 5.624\varepsilon(x)^2 \text{ for } \varepsilon\left(x\right) < 0, \tag{3}$$

$$P_{pz}^{AlN} = -1.808\varepsilon\left(x\right) - 7.888\varepsilon(x)^2 \text{ for } \varepsilon\left(x\right) > 0$$

$$P_{pz}^{GaN} = -0.918\varepsilon\left(x\right) + 9.541\varepsilon(x)^2 \tag{4}$$

$$\varepsilon\ (x) = \left[a_0 - a\left(x\right)\right]/a\left(x\right) \tag{5}$$

TABLE I
DENSITIES (σ) OF SHEET CHARGES AT INTERFACES I_1, I_2, I_3, AND I_4, THE EFFECTIVE BARRIER HEIGHTS FOR ELECTRONS ($\Delta\Phi_E$), THE EFFECTIVE BARRIER HEIGHTS FOR HOLES ($\Delta\Phi_H$), AND THE BARRIER HEIGHT AT THE INSERTED $Al_XGa_{1-X}N$/P-EBL INTERFACE (Φ_0) FOR SAMPLES A, B, AND C

Device number	Sample A	Sample B	Sample C
σ_i (m^{-2})	8.5 ×10^{15} (σ_1)	5.5 ×10^{16} (σ_2)/ -4.7 ×10^{16} (σ_3)	-4.7 ×10^{16} (σ_4)
$\Delta\Phi_e$ (meV)	368.9	388.2	830.5
$\Delta\Phi_h$ (meV)	470.3	396.4	279.4
Φ_0 (meV)	/	193.1	192.3

In equation (5), a_0 and $a(x)$ are the lattice constant of the substrate and the $Al_xGa_{1-x}N$ layer, respectively. The relevant material parameters of AlN and GaN can be found in Refs [35], [36]. The density of sheet charges at the heterointerface can be calculated by:

$$\sigma = \frac{\{P_{sp}\,(bottom)+P_{pz}\,(bottom)\}-\{P_{sp}\,(top)+P_{pz}\,(top)\}}{q} * \alpha \tag{6}$$

where q is the elementary charge and α is the polarization level of AlGaN ternary alloy, which is set to be 0.4 in the simulation process to account for the screening effect on the polarization by the defects and dislocations [27], [37]. The values of calculated σ are marked in Table I. And the values of the effective barrier heights for electrons, the effective barrier heights for holes, and the barrier height at the inserted $Al_xGa_{1-x}N$/p-EBL interface are also displayed in Table I.

Fig. 3(a) displays the calculated energy band of Sample A. The positive sheet charges at interface I_1 will attract electrons to accumulate in the vicinity of the interface and give rise to the electron leakage. In addition, $\Delta\Phi_e$ and $\Delta\Phi_h$ are 368.9 meV and 470.3 meV for Sample A (see Table I), respectively. From Fig. 3(b) and Table I, we can see that the density of the positive sheet charges at interface I_2 for Sample B is larger than that at interface I_1 for Sample A. This can be attributed to the larger discrepancy of Al composition between the inserted $Al_{0.75}Ga_{0.25}N$ layer and the LQB than that between the p-EBL and the LQB. Thus, the positive sheet charges at interface I_2 will bend the energy band downwards to a greater extent for Sample B in contrast with Sample A. Therefore, more electrons are attracted and accumulated in the vicinity of interface I_2 and more electrons subsequently tend to overflow to p-type region. However, the effective barrier height for electrons for Sample B is increased to 388.2 meV, which will help to hinder electrons from overflowing into p-type region. Besides, the negative sheet charges generated at interface I_3 can reflect the overflowed electrons back to the active region and simultaneously attract more holes into p-EBL from p-type hole supplier. Fig. 3(c) shows the energy band of Sample C with an $Al_{0.57\sim0.75}Ga_{0.43\sim0.25}N$ layer inserted between the LQB and p-EBL. There exist the same amount of negative sheet charges at interface I_4 of Sample C as Sample B, and thus the overflowed electrons will be reflected to the MQW

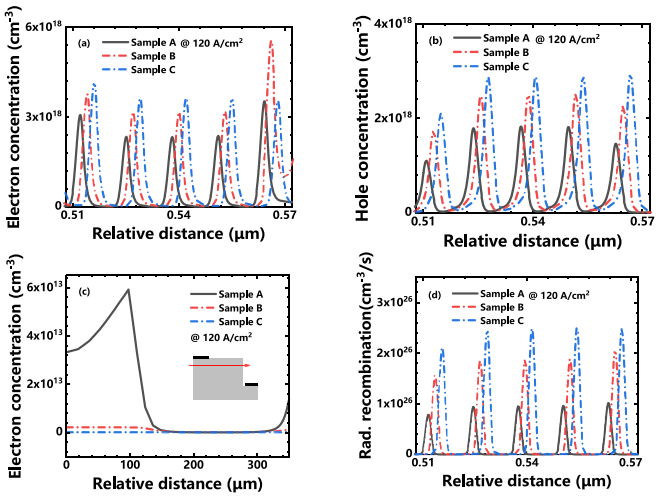

Fig. 4. (a) Electron concentration and (b) Hole concentration in MQW region at an injection current density of 120 A/cm^2 of Samples A, B, and C. (c) Horizontal electron concentration distribution profiles in the p-$Al_{0.4}Ga_{0.6}N$ layer of Samples A, B and C under 120 A/cm^2. The inset figure displays the position along which the electron distribution profile is captured. (d) Radiative recombination rates in MQW region under 120 A/cm^2 of Samples A, B, and C. Note that the horizontal positions of electron concentration, hole concentration, and radiative recombination rates in MQW region are shifted 2 nm and 4 nm for Sample B and Sample C, respectively, to make a clearer comparison.

region and holes can be accumulated in the vicinity of interface I_4. Nevertheless, no positive sheet charges are generated at the LQB/$Al_{0.57\sim0.75}Ga_{0.43\sim0.25}N$ interface because the LQB and the beginning of $Al_{0.57\sim0.75}Ga_{0.43\sim0.25}N$ layer possess the same Al composition. Hence, the energy band in the vicinity of the LQB/$Al_{0.57\sim0.75}Ga_{0.43\sim0.25}N$ interface is bent upwards, resulting in electron depletion, which is unfavorable for electron overflow. Moreover, the effective barrier height for electrons is significantly increased from 388.2 meV for Sample B to 830.5 meV for Sample C (see Table I). Due to these advantages, the electron leakage of Sample C can be further suppressed, compared with Sample B. Fig. 3(d) shows the hole concentration in p-EBL of the three samples. The positive sheet charges will deplete the holes near interface I_1, and this depletion effect leads to a low hole concentration in p-EBL of Sample A, which is detrimental to the hole injection efficiency into MQW region. Besides, it can be observed that the hole concentration profiles in p-EBL for Sample B and Sample C are nearly identical, which can be attributed to the same amount of negative sheet charges at interface I_3 and I_4, respectively.

For the purpose of verifying the effects of the inserted structure on the performance of DUV LEDs, we plotted the electron and hole distribution profiles in MQW region of all the investigated devices at an injection current density of 120 A/cm^2, as presented in Fig. 4(a) and (b). To make a clearer comparison, the horizontal positions of electron and hole concentration are shifted 2 nm and 4 nm severally for Sample B and Sample C. It can be observed that the electron concentration in MQW region of Sample B and Sample C is higher than that of Sample A. The enhanced electron confinement of the active region can be attributed to the increased $\Delta\Phi_e$ of Sample B and Sample C (see Table I) and the reflection of the negative sheet charges at the inserted $Al_xGa_{1-x}N$/p-EBL interface. The relatively larger $\Delta\Phi_e$ and the electron depletion near the LQB/$Al_{0.57\sim0.75}Ga_{0.43\sim0.25}N$ interface due to the vanishment of positive sheet charges together lead to a better electron confinement of Sample C than Sample B. It is notable that the electron concentration in the last quantum well of Sample B is the highest, which arises from the electron accumulation caused by the positive sheet charges at the LQB/$Al_{0.75}Ga_{0.25}N$ interface. Similarly, the decreased $\Delta\Phi_h$ and increased hole concentration in p-EBL contribute to the boosted hole concentration in the active region of Sample B and Sample C, which can be observed in Fig. 4(b). Because the $\Delta\Phi_h$ and Φ_0 of Sample C are smaller than those of Sample B, holes can be injected more easily from p-type region into the MQW region and consequently Sample C possesses higher hole concentration in the MQW region. Furthermore, the electron and hole distribution profiles in the active region of Sample C are both more uniform than those of Sample A and Sample B, which is beneficial to radiative recombination.

Fig. 4(c) shows the horizontal electron distribution profiles in the p-$Al_{0.4}Ga_{0.6}N$ layer for all the studied devices at 120 A/cm^2. It can be seen that the overall electron leakage of Sample B is suppressed due to its higher $\Delta\Phi_e$ than Sample A, yet Sample C exhibits a further alleviated electron leakage because of its significantly higher $\Delta\Phi_e$ than Sample B and the electron depletion due to the absence of positive sheet charges at the LQB/$Al_{0.57\sim0.75}Ga_{0.43\sim0.25}N$ interface. The significantly suppressed electron leakage can contribute to the obviously mitigated efficiency droop for the proposed DUV LEDs [16], [38], [39], as shown in Fig. 2(b). The enhanced electron and hole concentration in MQW region and suppressed electron leakage lead to nearly twice radiative recombination rates for Sample B compared to Sample A, as shown in Fig. 4(d). Moreover, Sample C exhibits nearly threefold radiative recombination rates than Sample A, benefiting from its highest electron concentration, hole concentration, and the lowest electron leakage.

IV. Conclusion

To conclude, we propose a DUV LED with an Al-composition-increasing AlGaN layer inserted at the LQB/p-EBL interface to promote the carrier injection efficiency, obtaining undamaged forward voltage at the same time. Besides, we numerically analyzed the mechanism of boosting the carrier injection by inserting an Al-rich AlGaN layer or an ACI-AlGaN layer between the LQB and the p-EBL. On the one hand, DUV LED with an ACI-AlGaN layer can eliminate the positive sheet charges at the LQB/ACI-AlGaN interface, which can form electron depletion in the vicinity of this interface, reducing the electron leakage into p-type region. On the other hand, this inserted structure can introduce negative sheet charges at the ACI-AlGaN/p-EBL interface, which will help to reflect overflowed electrons back into MQW region and induce hole accumulation in p-EBL simultaneously. The comparison of carrier concentration, EQE, optical power, and radiative recombination rates among the three devices suggested that the DUV LED with an ACI-AlGaN layer inserted at the LQB/p-EBL interface can

obtain boosted and homogenized carrier (including electron and hole) concentration in the MQW region and thus outstanding performance among the three devices. Therefore, the inserted ACI-AlGaN layer provides an alternative approach to enhance the carrier injection and confinement and achieve DUV LEDs with high EQE and optical power.

ACKNOWLEDGMENT

The authors thank staff from Simucal Inc., Yongchen Ji and Hang Zhou from School of Microelectronics, Shandong University, and Changsheng Xia from Sinopeda Technology Company Ltd. for their fruitful discussion.

REFERENCES

[1] M. Kneissl, T. Y. Seong, J. Han, and H. Amano, "The emergence and prospects of deep-ultraviolet light-emitting diode technologies," *Nat. Photon.*, vol. 13, no. 4, pp. 233–244, Apr. 2019.

[2] A. Khan, K. Balakrishnan, and T. Katona, "Ultraviolet light-emitting diodes based on group three nitrides," *Nat. Photon.*, vol. 2, no. 2, pp. 77–84, Feb. 2008.

[3] Z. Ren *et al.*, "Band engineering of III-nitride-based deep-ultraviolet light-emitting diodes: A review," *J. Phys. D: Appl. Phys.*, vol. 53, no. 7, Feb. 2020, Art. no. 073002.

[4] H. Hirayama, N. Maeda, S. Fujikawa, S. Toyoda, and N. Kamata, "Recent progress and future prospects of algan-based high-efficiency deep-ultraviolet light-emitting diodes," *Jpn. J. Appl. Phys.*, vol. 53, no. 10, Oct. 2014, Art. no. 100209.

[5] S.-I. Inoue, T. Naoki, T. Kinoshita, T. Obata, and H. Yanagi, "Light extraction enhancement of 265 nm deep-ultraviolet light-emitting diodes with over 90 mW output power via an AlN hybrid nanostructure," *Appl. Phys. Lett.*, vol. 106, no. 13, Mar. 2015, Art. no. 131104.

[6] W. Wang *et al.*, "Is a thin p-GaN layer possible for making high-efficiency algan-based deep-ultraviolet light-emitting diodes?," *Opt. Exp.*, vol. 29, no. 19, pp. 29651–29660, Sep. 2021.

[7] H. Sun *et al.*, "Unambiguously enhanced ultraviolet luminescence of AlGaN wavy quantum well structures grown on large misoriented sapphire substrate," *Adv. Funct. Mater.*, vol. 29, no. 48, Nov. 2019, Art. no. 1905445.

[8] Q. Chen *et al.*, "Improved the algan-based ultraviolet LEDs performance with super-lattice structure last barrier," *IEEE Photon. J.*, vol. 10, no. 4, Aug. 2018, Art. no. 8201007.

[9] J. Y. Chang, B. T. Liou, M. F. Huang, Y. H. Shih, F. M. Chen, and Y. K. Kuo, "High-efficiency deep-ultraviolet light-emitting diodes with efficient carrier confinement and high light extraction," *IEEE Trans. Electron Devices*, vol. 66, no. 2, pp. 976–982, Feb. 2019.

[10] C. Y. Huang *et al.*, "High-quality and highly-transparent AlN template on annealed sputter-deposited AlN buffer layer for deep ultra-violet light-emitting diodes," *AIP Adv.*, vol. 7, no. 5, May 2017, Art. no. 055110.

[11] J. Y. Chang, H. T. Chang, Y. H. Shih, F. M. Chen, M. F. Huang, and Y. K. Kuo, "Efficient carrier confinement in deep-ultraviolet light-emitting diodes with composition graded configuration," *IEEE Trans. Electron Devices*, vol. 64, no. 12, pp. 4980–4984, Dec. 2017.

[12] B. T. Tran and H. Hirayama, "Growth and fabrication of high external quantum efficiency algan-based deep ultraviolet light-emitting diode grown on pattern si substrate," *Sci. Rep.*, vol. 7, Sep. 2017, Art. no. 12176.

[13] K. Li, N. Zeng, F. Liao, and Y. Yin, "Investigations on deep ultraviolet light-emitting diodes with quaternary AlInGaN streamlined quantum barriers for reducing polarization effect," *Superlattices Microstruct.*, vol. 145, Sep. 2020, Art. no. 106601.

[14] A. Pandey, W. J. Shin, J. Gim, R. Hovden, and Z. Mi, "High-efficiency AlGaN/GaN/AlGaN tunnel junction ultraviolet light-emitting diodes," *Photon. Res.*, vol. 8, no. 3, pp. 331–337, Mar. 2020.

[15] S.-I. Inoue, N. Tamari, and M. Taniguchi, "150 mW deep-ultraviolet light-emitting diodes with large-area AlN nanophotonic light-extraction structure emitting at 265 nm," *Appl. Phys. Lett.*, vol. 110, no. 14, Apr. 2017, Art. no. 141106.

[16] C. Chu *et al.*, "On the impact of electron leakage on the efficiency droop for AlGaN based deep ultraviolet light emitting diodes," *IEEE Photon. J.*, vol. 12, no. 3, Jun. 2020, Art. no. 1600207.

[17] M. N. Sharif, M. I. Niass, J. J. Liou, F. Wang, and Y. Liu, "p-AlInN electron blocking layer for algan-based deep-ultraviolet light-emitting diode," *Superlattices Microstruct.*, vol. 158, Oct. 2021, Art. no. 107022.

[18] Z. H. Zhang *et al.*, "UVA light-emitting diode grown on si substrate with enhanced electron and hole injections," *Opt. Lett.*, vol. 42, no. 21, pp. 4533–4536, Nov. 2017.

[19] C. Chu *et al.*, "On the origin of enhanced hole injection for algan-based deep ultraviolet light-emitting diodes with AlN insertion layer in p-electron blocking layer," *Opt. Exp.*, vol. 27, no. 12, pp. A620–A628, Jun. 2019.

[20] L. Li, Y. Miyachi, M. Miyoshi, and T. Egawa, "Ultrathin inserted AlGaN/InAlN heterojunction for performance improvement in algan-based deep ultraviolet light-emitting diodes," *Appl. Phys. Exp.*, vol. 12, no. 1, Jan. 2019, Art. no. 011010.

[21] S. Wang, Y. A. Yin, H. Gu, N. Wang, and L. Liu, "Graded AlGaN/AlGaN superlattice insert layer improved performance of algan-based deep ultraviolet light-emitting diodes," *J. Display Technol.*, vol. 12, no. 10, pp. 1112–1116, Oct. 2016.

[22] X. Wang, H.-Q. Sun, and Z.-Y. Guo, "Improvement of algan-based deep ultraviolet light-emitting diodes by using a graded AlGaN superlattice hole reservoir layer," *Opt. Mater.*, vol. 86, pp. 133–137, Dec. 2018.

[23] M. Liu, Y. Ji, H. Zhou, C. Xia, Z. Zhang, and C. Liu, "Sheet charge engineering towards an efficient hole injection in 290 nm deep ultraviolet light-emitting diodes," *IEEE Photon. J.*, vol. 13, no. 4, Aug. 2021, Art. no. 8200308.

[24] T. Kolbe *et al.*, "Improved injection efficiency in 290 nm light emitting diodes with Al(Ga)N electron blocking heterostructure," *Appl. Phys. Lett.*, vol. 103, no. 3, Jul. 2013, Art. no. 031109.

[25] A. Al-Tawhid *et al.*, "Weak localization and dimensional crossover in compositionally graded $al_xGa_{1-x}n$," *Appl. Phys. Lett.*, vol. 118, no. 8, Feb. 2021, Art. no. 082101.

[26] A. M. Armstrong and A. A. Allerman, "Polarization-induced electrical conductivity in ultra-wide band gap AlGaN alloys," *Appl. Phys. Lett.*, vol. 109, no. 22, Nov. 2016, Art. no. 222101.

[27] D. Zhang *et al.*, "Improving hole injection from p-EBL down to the end of active region by simply playing with polarization effect for AlGaN based DUV light-emitting diodes," *AIP Adv.*, vol. 10, no. 6, Jun. 2020, Art. no. 065032.

[28] Accessed: Jun. 2019. [Online]. Available: http://www.crosslight.com/

[29] Q. Chen *et al.*, "Improved the algan-Based ultraviolet LEDs performance with super-lattice structure last barrier," *IEEE Photon. J.*, vol. 10, no. 4, Aug. 2018, Art. no. 8201007.

[30] M. Kneissl, "A brief review of III-Nitride UV emitter technologies and their applications," in *III-Nitride Ultraviolet Emitters*, Cham, Switzerland: Springer, 2016, ch. 1, pp. 1–25.

[31] E. Kioupakis, P. Rinke, K. T. Delaney, and C. G. Van de Walle, "Indirect auger recombination as a cause of efficiency droop in nitride light-emitting diodes," *Appl. Phys. Lett.*, vol. 98, no. 16, Apr. 2011, Art. no. 161107.

[32] S. H. Lin *et al.*, "Enhanced external quantum efficiencies of algan-based deep-UV LEDs using reflective passivation layer," *Opt. Exp.*, vol. 29, no. 23, pp. 37835–37844, Nov. 2021.

[33] J. Piprek, "Ultra-violet light-emitting diodes with quasi acceptor-free AlGaN polarization doping," *Opt. Quantum Electron.*, vol. 44, no. 3-5, pp. 67–73, Jun. 2012.

[34] V. Fiorentini, F. Bernardini, and O. Ambacher, "Evidence for nonlinear macroscopic polarization in III–V nitride alloy heterostructures," *Appl. Phys. Lett.*, vol. 80, no. 7, pp. 1204–1206, Feb. 2002.

[35] I. Vurgaftman and J. R. Meyer, "Band parameters for nitrogen-containing semiconductors," *J. Appl. Phys.*, vol. 94, no. 6, pp. 3675–3696, Sep. 2003.

[36] F. Bernardini, V. Fiorentini, and D. Vanderbilt, "Spontaneous polarization and piezoelectric constants of III-V nitrides," *Phys. Rev. B*, vol. 56, no. 16, pp. 10024–10027, Oct. 1997.

[37] K. Tian *et al.*, "On the polarization effect of the p-EBL/p-AlGaN/p-GaN structure for algan-based deep-ultraviolet light-emitting diodes," *Superlattices Microstruct,* vol. 122, pp. 280–285, Oct. 2018.

[38] Z.-H. Zhang *et al.*, "Nearly efficiency-droop-free algan-based ultraviolet light-emitting diodes with a specifically designed superlattice p-Type electron blocking layer for high mg doping efficiency," *Nanoscale Res. Lett.*, vol. 13, Apr. 2018, Art. no. 122.

[39] Z. Ju *et al.*, "Advantages of the blue InGaN/GaN light-emitting diodes with an AlGaN/GaN/AlGaN quantum well structured electron blocking layer," *ACS Photon.*, vol. 1, no. 4, pp. 377–381, Apr. 2014.